Journal of Solid State Chemistry **145,** 317–326 (1999)
Article ID jssc.1999.8279, available online at http://www.idealibrary.com on IDEAL®

Reaction Sintering Process in Granular Composites: Application to a Superconductor/Ferrite System

Agnieszka Kopia-Zastawa,*,† Jean-Raymond Gavarri,*,[1] Ireneusz Suliga,† Marie-Angèle Fremy,* Marie-Hélène Pischedda,* and Stanislawa Jasienska†

*Laboratoire des Matériaux Multiphasés et Interfaces, UPRES 21 35, Faculté des Sciences et Techniques, Université de Toulon-Var, BP 132, 83 957 La Garde, France; and †Faculty of Metallurgy and Sciences of Materials, Academy of Mining and Metallurgy, 30, Al. Mickiewicza, 30 059, Krakow, Poland

Received December 16, 1998; in revised form March 9, 1999; accepted March 13, 1999

Granular superconductor–ferrite (*S*/*F*) composites have been fabricated using various sintering conditions (volume fraction Φ_0 of ferrite, volume fraction Σ_0 of superconductor, sintering temperature T_{sint}, sintering time t_{sint}). The superconducting *S* phase is the well-known Bi (Pb)–2223 phase ($T_c = 110$ K). The ferrite (*F*) is $NiFe_2O_4$. The reaction sintering process is experimentally described by determining the volume fractions of residual *S* and *F* phases from X-ray diffraction experiments. Magnetic measurements are used to analyze the degradation process in both residual ferrite and superconducting phases. Nonlinear evolutions of the Σ and Φ residual volume fractions as a function of initial compositions are observed. To interpret these results, we propose to express the chemical kinetics using two elemental reactions such as: $F+n.\ S \rightarrow P$ and $S+S \rightarrow P'$. Using various types of kinetics parameters, the solid state reaction in each composite can be modeled as a function of the initial Σ_0 and Φ_0 volume fractions. © 1999 Academic Press

Keywords: **high T_C superconductors; ferrite–superconductor composites; bismuth cuprate superconductors; reaction sintering process; chemical kinetics; degradation; modeling.**

I. INTRODUCTION

For several years, various reinforced superconducting ceramics have been envisaged (1–20): ceramics enveloped by metallic shells (tubes) or granular ceramics in which additions are inserted. In all cases, the additions take part in the conducting process of the whole element.

In their studies of metal–superconductor or oxide–superconductor composites (21–23), the authors studied and modeled the percolation of superconducting currents as a function of temperature, composition, and sintering process. In our own studies (24–26), we established relations between the sintering process and the final superconducting properties of composite pellets.

Generally, to keep the superconducting properties, the additional constituents have to be chemically inert in the presence of the ceramics. However, in the case of bismuth cuprate superconductors, such as the $Bi_{2-x}Pb_xSr_2Ca_2Cu_3O_{10-x}$ phase (Bi-2223, $T_c = 110$ K), the "(Bi,Pb)SrCaCuO" phases are generally highly reactive or unstable. These bismuth cuprate phases react with many metals and oxides; as a consequence, their superconducting properties are subjected to a systematic degradation. For these reasons, a lot of works have been carried out using noble metallic additions or substrates like Au, Pt, Ag, as well as Cu and Ni (4, 8–10), or using polymer matrix (27–30) in the case of the bismuth cuprate superconductors.

In our previous work (31), we studied the chemical evolution of composite materials obtained from the superconducting bismuth cuprate $Bi_{2-x}Pb_xSr_2Ca_2Cu_3O_{10-x}$ (Bi-2223, $T_c = 110$ K) and stainless steel grains. Given its initial resistance to corrosion and its high elastic properties, stainless steel was chosen as an interesting candidate to try to improve the mechanical and the elastic properties of superconducting pellets.

The general aim of the present work is to elaborate and study a granular composite presenting two types of properties: superconductivity (at low temperature) and ferromagnetism (at low or room temperature).

The superconducting properties are delivered by the well-known high T_c superconducting ceramics Bi-2223 ($T_c = 110$ K). The ferromagnetic behavior is delivered by a ferrite, $NiFe_2O_4$, well known in wave-guide applications. Below a certain transition temperature (T_c), superconducting currents can occur either in individual ceramics grains or through the whole sample when Josephson junctions are well formed. When the composite is subjected to an external magnetic field, two types of interactions can be expected: first, the magnetic field could be expelled from the superconducting grains; second, the ferromagnetic components should interact with this field and, as a consequence, exert an action on the neighboring superconducting currents. So,

[1] To whom correspondence should be addressed.

0022-4596/99 $30.00

two different types of applications might be concerned: the screening or "wave-guide" applications and the detection of magnetic fields.

Two types of composites might be considered: either sandwiches or granular pellets. In this study, we only deal with granular composites to analyze the reciprocal influences of a superconducting phase and of a ferrite as a function of their volume fractions and of a given sintering process.

In fact three types of problems must be solved:

1. the relative influences of each phase on the propagation of the magnetic fields
2. the influences on properties of interphase growing and chemical diffusion due to the sintering processes
3. the possibility of preparing such granular composites with a good cohesion and good mechanical properties, without destroying each phase.

It is necessary to recall here that to restore the Josephson junctions and to create some cohesion between grains, the elaboration process will systematically involve chemical diffusion and degradation. So, to obtain interesting final properties, it is necessary to better understand the chemical reactivity at the interfaces in such two-phase active composites.

We have chosen to prepare such composites from powders of bismuth cuprate Bi-2223 and from powders of $NiFe_2O_4$ ferrite (saturation magnetic field $H = 3000$ Gauss). The H_{c1} of the bismuth cuprate is about 100 to 200 Gauss following the ceramics preparation. Thus, the influence of the ferrite is expected to be strong, following its own magnetization in the presence of an external field.

II. EXPERIMENTAL PART

II.1. Sample Preparation

The superconducting phase was an Aldrich powder of bismuth cuprate Bi-2223 ($Bi_{1,6}Pb_{0,4}Sr_2Ca_2Cu_3O_{10+x}$), having a standard "offset" T_c of 110 K. The ferrite was a commercial powder of $NiFe_2O_4$, obtained from a Polish industry specializing in magnetic materials (Zaklady Materialow Magnetycznych POLFER).

The initial average sizes were controlled using a Malvern Sizer laser granulometer (0.3 to 300 μm); the mean linear diameters were found to be 18.7 μm for the Bi-2223 powder and 28.8 μm for the ferrite powder.

Two types of samples were prepared: initial composites were first prepared by compressing mixtures of powders with variable volume fractions under 5 kbar to obtain pellets of about 13 mm of diameter and 1 to 2 mm of thickness. Then other identical series of pellets were prepared and the samples were sintered using various sintering temperatures (in the range 800 to 830°C) and sintering times (5 to 30 min.).

Each sample was then subjected to systematic analyses to characterize the phases and the variable properties.

TABLE 1
Volume Fractions of Ferrite and Superconductor in the Composite Pellets before Sintering

Φ_{fer} [× 100] before sintering	Φ_{fer}[× 100] after sintering	Φ_{por}[× 100] after sintering	Σ_{sup}[× 100] after sintering
0	0	16.92	83.08
5	3.85	22.83	73.32
10	8.15	18.45	73.4
15	12.09	19.30	68.61
20	15.20	23.94	60.86
25	21.34	14.6	64.06
30	23.7	20.98	55.32
35	29.51	15.67	55.82
40	35.98	10.00	54.02
45	35.55	20.98	43.47
50	43.45	13.07	43.48
60	50.7	15.49	33.81
70	64.52	7.81	27.67
80	67.60	15.49	16.91
85	68.95	18.87	12.18
100	82.75	17.25	0

Note. $\Phi_{fer} + \Phi_{por} + \Sigma_{sup} = 1$ before sintering.

In Table 1 the various composites are listed with their initial volume fractions (calculated from the densities of the phases), their effective volume fraction (measured from the volume of each pellet), and the volume fraction of the cavities.

In Table 2, the composite samples obtained after sintering are listed.

TABLE 2
Sintering Conditions and Notations of the Sintered Composites

	Notation: ST [°C] − t [min.] − Φ [× 100]		
T →	800	820	830
Composited: S (T[°C], t [min], Φ[× 100])	S800-5-20; S800-10-20; S800-20-20; S800-30-20	S820-5-20; S820-10-20; S800-10-25; S800-10-30;	
	S800-30-0	S820-20-20	
	S800-30-5	S820-30-0	S830-30-0
	S800-30-10	S820-30-5	S830-20-10
	S800-30-15	S820-30-15	S830-30-15
	S800-30-20	S820-30-20	S830-30-20
	S800-30-25	S820-30-25	S830-30-25
	S800-30-30	S820-30-30	S830-30-30
	S800-30-40	S820-30-40	S830-30-40
	S800-30-50	S820-30-50	S830-30-60
	S800-30-60	S820-30-60	S830-30-70
	S800-30-70	S820-30-70	S830-30-80
	S800-30-80	S820-30-80	S830-30-90
	S800-30-90	S820-30-90	S830-30-100
	S800-30-90	S810-30-90	
	S800-30-100	S820-30-100	

Caption for sample notations: S820-30-15 = Sample for (T,t,100Φ)

II.2. X-Ray Diffraction Analysis

The pellets were characterized by X-ray diffraction using a D5000-Siemens diffractometer equipped with a Cu anticathode (experimental conditions: 35 kV, 30 mA, Ni filter, 2θ angle range: 3 to 65 degrees). The two initial phases were used as standards to analyze the composites after the sintering process. The intensity of Bragg peaks has been used to characterize the evolution of phases after sintering.

II.3. Levitation Device

The magnetic field interaction of each sample was then first analyzed using a homemade levitation device previously described in (27, 28). Each composite pellet interacts with a cylindrical magnet of Nd–Fe–B from UGIMAG (Grenoble). When the composite is cooled down to liquid nitrogen temperature, two effects occur:

1. the attraction due to magnetization of ferrite grains
2. the magnetic field expulsion due to superconducting grains.

In addition the effect of magnetization of ferrite can play a role in the effective response of the superconducting grains (which are type II superconductors). Finally, for sintered samples, the degradation of both phases that can occur during the sintering process can be analyzed from the abnormal magnetic response.

The levitation forces (**F**) are sensitive to magnetic field penetration in the composite; obviously in such measurements the face of the pellet which is in front of the magnet plays a prominent role in the interaction.

II.4. Susceptibility Measurements

Susceptibility measurements (χ) were carried out using a homemade device allowing us to record the magnetic responses down to 20 K.

In such analyses the composite is first ground, so the magnetic response characterizes the volume of the sample, which is not the case of the levitation measurements.

Generally, the χ curves can be characterized as a function of temperature by:

- their value at 300 K (noted H) and the slope $d\chi/dT$ above the transition temperature T_c, which both depend on the ferromagnetic components;
- their onset temperatures T_c (two T_c temperatures can be observed according to the presence of a second superconducting phase);
- the χ value at very low temperature (about 20 K), which can be directly connected with the proportion of residual superconducting phase after sintering process and in the presence of ferrite components; in fact, to better determine such a residual S phase, we have to consider the difference noted, X_{obs}, between the χ value observed at 20 K (superconducting Bi phase) and the χ value extrapolated from the χ evolution observed for $T > T_c$ (normal Bi phase).

It is important to note that our susceptibility data are mainly representative of the individual grains in our experiments.

II.5. Scanning Electron Microscopy (SEM)

A scanning electron microscopy analysis was carried out using PHILIPS XL 30 equipment to characterize the morphology and distribution of the phases before and after sintering. EDAX analysis was used to determine the composition of each phase.

III. RESULTS

III.1. X-Ray Diffraction Analysis

Standard samples. To standardize our experiments, a series of just-compacted composites obtained without any thermal treatment has been analyzed by X-ray diffraction; the analysis of the normalized Bragg peak intensities has shown linear variations of these intensities as the fraction Φ of ferrite varies, in the full volume fraction range. Thus, each intensity evolution observed in the various sintered samples can be correlated to the sole degradation of each phase.

Texture effects. In addition, using electron microscopy observations and the X-ray diffraction data, we have verified that the texture (grain orientations) of the plane surfaces of our sintered composites is not affected by the sintering process and does not vary with the composition.

Sintered samples. The X-ray diffraction patterns reported in Figs. 1a–1c show that the effect of sintering is related to a degradation reaction of both phases with a stronger degradation in the case of the cuprate. In Fig. 2, the evolutions of the normalized Bragg peak intensities of the Bi-2223 phase and of the ferrite phase are represented for each sintering temperature (800, 820, and 830°C).

The normalized intensities noted I^N are assumed to deliver the volume fractions and are obtained as:

$$I^N_{Bi\text{-}2223} = S_{s[00\underline{10}]}/S^0_{Bi\text{-}2223}$$

$$I^N_{NiFe204} = S_{s[311]}/S^0_{NiFe204}$$

where $I^N_{Bi\text{-}2223}$ is the normalized surface under the Bi2223 [00$\underline{10}$] Bragg peak for the composites; $S_{s[00\underline{10}]}$ is the surface under the Bi2223 [00$\underline{10}$] peak for the composites (S–T–t–Φ); $S^0_{Bi\text{-}2223}$ is the surface under the Bi2223 [00$\underline{10}$] peak for the pure S sample; $I^N_{NiFe204}$ is the normalized surface under the $NiFe_2O_4$ [311] Bragg peak for the composites; $S_{s[311]}$ is the surface under the $NiFe_2O_4$ [311] peak for the composites

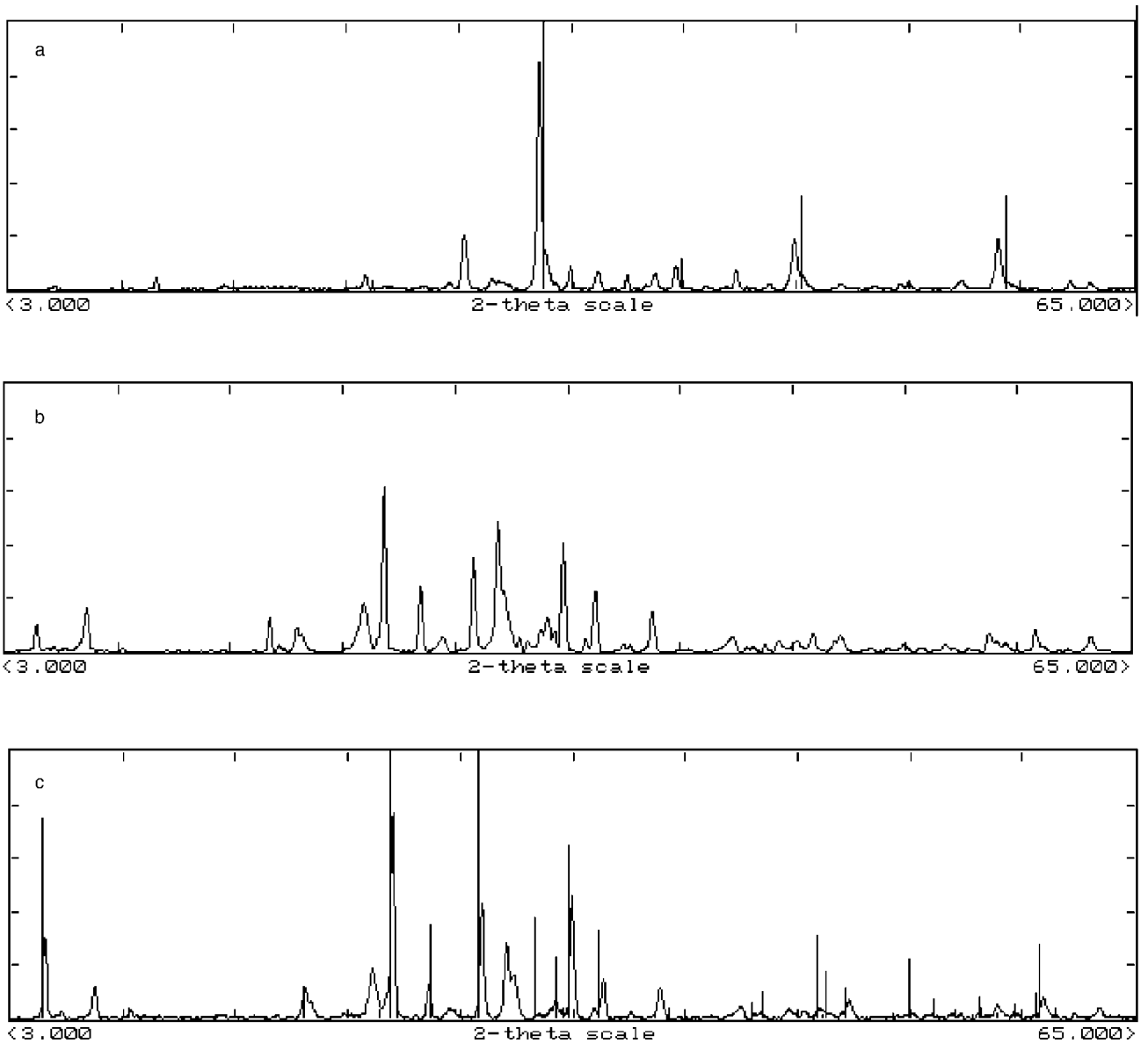

FIG. 1. X-ray diffraction pattern of a composite showing the presence of a $SrFeO_3$ phase with the initial phases (Bi-2223/$NiFe_2O_4$). The intensities have been measured in order to determine the *S* and *F* final volume fractions using standardized patterns. The $SrFeO_3$ phase has been partly confirmed from SEM experiments at the interfaces ferrite–superconductor as thin barriers. (a) S830-30-40, $T = 830°C$; (b) S820-30-40, $T = 820°C$; (c) S800-30-40, $T = 800°C$.

(S–T–t–Φ); and $S^0_{NiFe204}$ is the surface under the $NiFe_2O_4$ [311] peak for the pure *F* sample.

Considering these curves as representative of the residual fractions of *S* and *F* phases after sintering, it should be noted that the degradation of each phase is not linear: for the *S* phase an apparent "critical" volume fraction could be defined by extrapolation on the graphs.

Apparition of unusual phases. In addition, in the case of samples having a high ferrite content, the growing of new phases has been evidenced. A refinement of the cell parameters has shown that one of these phases might be the $SrFeO_{3-x}$ phase (Fig. 1a; JCPDS No. 34-0641, 40-0906).

This $SrFeO_3$ phase has been strongly suggested from the SEM experiments and located at the interfaces ferrite–superconductor as thin barriers. However, more detailed analyses are needed to ensure the exact composition of such phases which should involve oxidation states of iron in the solid state higher than the current 3^+ degree.

The Bi-2201 (JCPDS No. 42-0241) and CuO (JCPDS No. 45-0937) well-known phases are systematically observed (Figs. 1b and 1c).

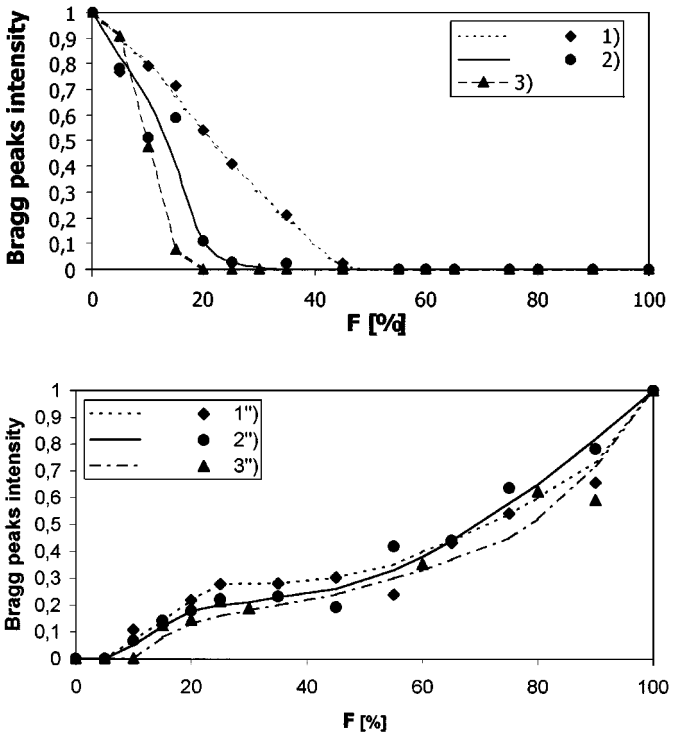

FIG. 2. Bragg peak intensities. Up curve: I(Bi-2223); Down curve: I($NiFe_2O_4$). Normalized Intensities of Bragg peaks at 800, 820 and 830°C as a function of the volume fraction Φ of ferrite. The vanishing of the *S* phase (up) is respectively observed at $\Phi_{lim} = 0.50$, 0.35, 0.20 as the temperature increases. The degradation of the *F* phase is clearly observed at 830°C.

III.2. Magnetic Interaction Analysis and Levitation Effects

In Fig. 3, the experimental forces obtained at room temperature ($\mathbf{F}_{tot} = \mathbf{F}_{ferr}$ only) and at the temperature of liquid N_2 ($\mathbf{F}_{tot} = \mathbf{F}_{ferr} + \mathbf{F}_{lev}$) are reported. The repulsion force $\mathbf{F}_{lev}$ due to the superconductor is strongly compensated by the attraction force $\mathbf{F}_{ferr}$ due to the ferrite when the volume fraction of ferrite increases.

In the case of the S800 samples (Fig. 3a) a zero value of the total force $\mathbf{F}_{tot} = \mathbf{F}_{lev} + \mathbf{F}_{ferr}$ is obtained at $\Phi = 0.05$ and the general $\mathbf{F}_{tot}$ evolutions at $T < T_c$ and $T = 300$ K are roughly linear. However a small anomaly should be observed in the 0.30 to 0.70 composition Φ range.

In the case of the S820 samples, an anomaly in the $\mathbf{F}_{tot}$ evolution is clearly observed in the 0.20 to 0.60 composition Φ range (Fig. 3b).

Finally, for the S830 samples an abnormal behavior is observed in the 0 to 0.40 composition range: this can be directly ascribed to the strong degradation of both S and F phases, which should have been thermally activated at 830°C. It should be noted that, in this last case, the degradation of the F phase seems to be more pronounced than the degradation of the S phase: in the 0 to 0.20 composition Φ range, we observe a residual superconducting signal at $T < T_c$ (close-up of Fig. 3c).

III.3. Susceptibility Measurements

In Figs 4a–4c, we have reported a series of susceptibility measurements corresponding to S800, S820, and S830 samples. The susceptibility data obtained on powders of sintered composites clearly show that, in our composites, a residual superconducting behavior is observed up to 40% of ferrite. Above this approximate composition, the superconducting state disappears. This is consistent with the interaction force evolutions of Figs. 3a–3c, at $T < T_c$ and $T > T_c$, in which we can observe the vanishing of any levitation force above 30–40% of ferrite. In addition the X-ray diffraction patterns show that the Bi-2223 phase is no longer present above 30–40% of ferrite.

From the data of Fig. 4, we have determined the values $H(\Phi, 300\text{ K}) = \chi$ at 300 K and the superconducting contribution $X(\Phi, 20\text{ K}) = \Delta\chi = \chi(\text{extrapolated}) - \chi(20\text{ K})$ for the same samples S800, S820, and S830. The extrapolated value χ(extrapolated) is obtained by extrapolating the linear variation observed between T_c and 300 K down to 20 K. In Figs. 5a–5c, we have reported the direct values $H(\Phi, 300\text{ K})$ and the normalized values $X = X(\Phi, 20\text{ K})/X(0, 20\text{ K})$. As it can be clearly observed, the variation of *H* is characteristic of the degradation of the ferrite phase while the variation of *X* is characteristic of the degradation of the superconducting phase. For both phases *S* and *F*, it should be noted that the amplitude of degradation can be directly evaluated from the differences between the experimental values *X* and $H(\Phi, 300\text{ K})$ and ideal *X* and *H* values that could have been obtained from hypothetical linear evolutions.

In the case of Fig. 5a (S800 samples) the evolutions of *H* and *X* show that the F phase is only weakly degraded while the *S* phase is partly degraded. In Fig. 5b, we observe a strong degradation of the *S* phase: this corroborates the analysis of the interaction forces and the analysis of the Bragg peaks. In Fig. 5c, a strong degradation of both *S* and *F* phases is clearly observed. This is in full agreement with the other observations reported above in the text: at 830°C, the degradation kinetics is strongly thermally activated. Correlatively, in the composition range 0.20 to 0.40, we observe that both ferrite and superconducting properties are fully degraded in these S830 samples.

Another feature has to be noted: at a fixed sintering temperature, the degradation of the *S* phase is systematically greater than that of the *F* phase.

All of these evolutions suggest that we could define a limit value of Φ_{lim} for the existence of the residual Bi-2223 phase obtained after sintering.

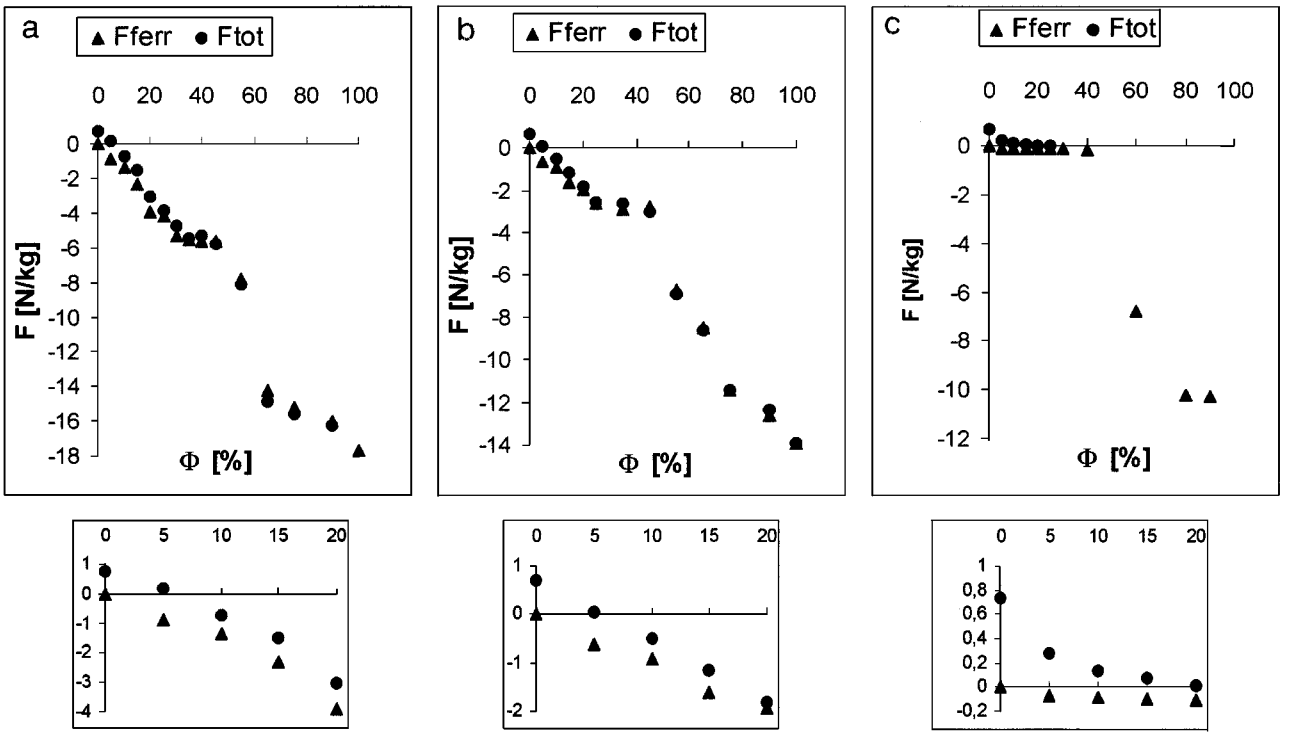

FIG. 3. Interaction forces **F** between the composite pellets and a magnet at room temperature and at 77 K (liquid nitrogen) as a function of the Φ vol. fraction. (a) S800-30-Φ samples: $\mathbf{F}_{tot}$ points are obtained at $T < T_c$, $\mathbf{F}_{ferr}$ points (triangles) are obtained at 300 K (only magnetic attraction of ferrite); the zoom shows the role of the repulsion component of the residual superconducting phase. (b) S820-30-Φ samples: $\mathbf{F}_{tot}$ points are obtained at $T < T_c$, $\mathbf{F}_{ferr}$ points (triangles) are obtained at 300 K (only magnetic attraction of ferrite); the zoom shows the role of the repulsion component of the residual superconducting phase; an anomaly is observed (departure from linear behavior). (c) S830-30-Φ samples: $\mathbf{F}_{tot}$ points are obtained at $T < T_c$, $\mathbf{F}_{ferr}$ points (triangles) are obtained at 300 K (only magnetic attraction of ferrite); the zoom shows the role of the repulsion component of the residual superconducting phase; a strong anomaly is observed in the 0 to 0.40 composition Φ range of ferrite. This is due to a thermally activated degradation of the system.

III.4. Scanning Electron Microscopy

In Figs. 6a–c, selected micrographs show the presence of one isolated ferrite grain around which a reaction is observed: in fact, the atoms of the superconducting phase seem to have migrated regularly all over the surface of the grain.

To confirm the XRD analyses presented above which suggested the existence of several new phases such as $SrFeO_{2.73}$ or $Bi_{3.11}Ca_{0.89}O_{5.56}$, a SEM analysis of the interphase regions between the Bi-2223 phase and ferrite grains was carried out in detail. These two phases have been qualitatively confirmed by this SEM analysis: they are observed as interphase barriers separating the superconducting cuprate phase from the ferrite grains. The EDAX analyses are congruent with the chemical compositions reported in the JCPDS library.

IV. DISCUSSION

As it can be clearly observed on the various curves, a first limit composition Φ_{lim} can be defined in the present multiphase system obtained after sintering: $T = 800°C$, $\Phi_{lim} = 0.50$; $T = 820°C$, $\Phi_{lim} = 0.35$; $T = 830°C$, $\Phi_{lim} = 0.23$, above which the superconducting behavior seems to fully vanish in our samples.

The XRD analyses show the vanishing of the Bi-2223 phase in the limit of the accuracy of our analysis. The levitation curves at room temperature and low temperature are similar above 25 or 30 vol% of ferrite. In the case of susceptibility curves the phase transition seems to exist again up to 30%.

Now, for a better understanding of the chemical evolution of our composite system, we present a first simplified approach using classical kinetics equations.

IV.1. Modeling

In order to interpret the chemical evolutions of our S/F composites, we propose to make use of various classical modeling approaches. The basic degradation of the S phase can be represented using two kinds of simplified reaction kinetics.

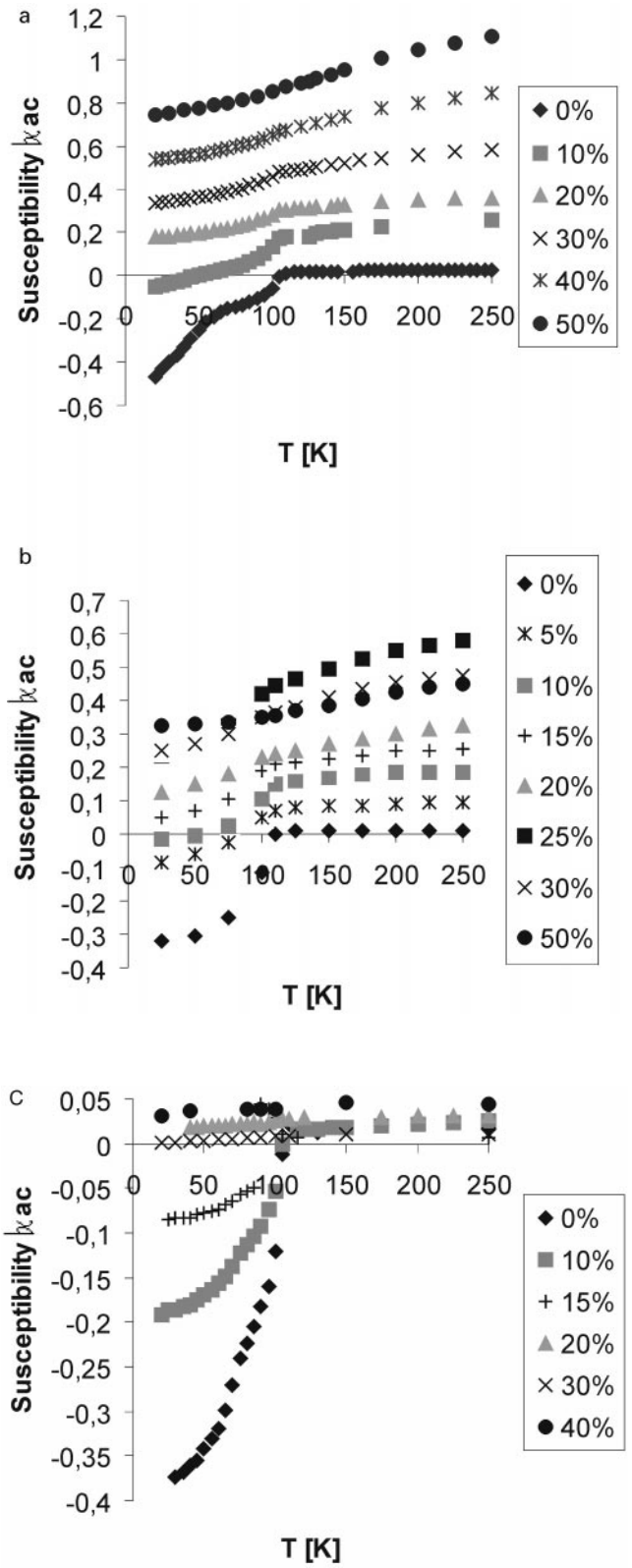

FIG. 4. A.C. Magnetic susceptibility measurements for S800 (a), S820 (b,) S830 (c) samples. The S800 samples are characterized by an abnormal signal for $\Phi = 0$ pure sample. This is linked with the formation of an other superconducting phase (Bi-2212, $T_c = 80$ K).

The first reaction assumes that the S and F phases (S and F grains) directly react together as

$$F + n.S \rightarrow P \qquad [1]$$

with a reaction rate: $v = -d[\Phi_I]/dt = k_1 . [\Sigma_I] . [\Phi_I]$.

The second reaction assumes that, at lower temperatures, the S phase decomposes into lemental components as suggested by the phase diagram (32)

$$S + S \rightarrow P' \qquad [2]$$

with a reaction rate associated with a second order reaction mechanism (well adapted to our present experiments):

$$v = -d[\Sigma_{II}]/dt = k_2 . [\Sigma_{II}]^2.$$

In these expressions, $[\Sigma_{I \text{ or } II}]$ and $[\Phi_{I \text{ or } II}]$ are the volume fractions of superconducting and ferrite phases, at time t and for kinetics (1) or (2). The factors k_1 and k_2 are generally thermally activated: $k_{1 \text{ or } 2} = k^0_{1 \text{ or } 2}$. $\exp(-E_{1 \text{ or } 2}/\mathrm{RT})$ where $E_{1 \text{ or } 2}$ are the activation energies of the process.

The n value is a parameter characteristic of the complex reactivity of our two-phase system. It can be justified as follows: given the weak stability of the Bi-2223 phase, the reaction might be described taking into account various successive reactions:

$$\text{Bi-2223} \rightarrow \text{Bi2212} + \text{“CaO} + \text{CuO”} \rightarrow \text{Bi2201} +$$

$$\text{“CaCuO2”} \rightarrow N \text{ final decomposition phases.}$$

Because of the lack of stability of the Bi-2223 phase (according to the phase diagram, it is stable only from 835 to 870°C), the second reaction can occur without any F addition. So, during the sintering process, the two types of reactions can occur. In the case of composites having weak F fractions, the second reaction might be prominent in the degradation process.

Finally, two types of solutions could be derived.

First solution (*Eq.* [1]): *S–F reaction.* After a certain time t, the fraction of degraded ferrite is noted x (x will be considered as a degradation fraction, n; x will be the degradation fraction of the S phase). The initial fractions being noted Σ_0 and Φ_0, the residual Σ_I and Φ_I fractions will be linked with the degradtion fraction x as follows: $\Sigma_I = \Sigma_0 - n$; x and $\Phi_I = \Phi_0 - x$. Then, the classical solution of Eq. [1] is

$$k_1 . t = [\Sigma_0 - n\Phi_0]^{-1} . \mathrm{Ln}[\Phi_0 . (\Sigma_0 - n.\ x)]/[\Sigma_0 \cdot (\Phi_0 - x)] \qquad [3]$$

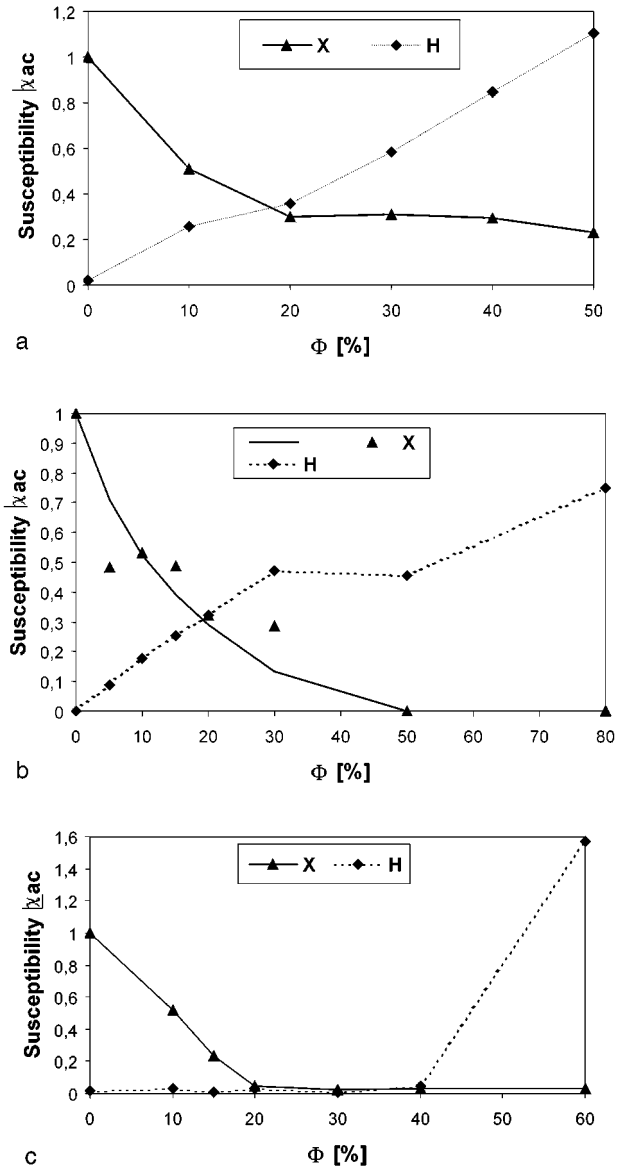

FIG. 5. Magnetic contributions of the *S* and *F* phases in the composites (S800, S820, S830): normalized *X* values due to the superconducting Meissner effect direct *H* values due to the ferrite phase at 300 K. In (c) a strong degradation of both *S* and *F* phases is observed (Φ range 0.20 to 0.40).

From this expression, we can obtain the function x:

$$x = [(K(t) - 1)/(K(t).\Sigma_0 - n.\ \Phi_0)].\ \Sigma_0.\ \Phi_0$$

$$K(t) = \exp[\Sigma_0 - n.\ \Phi_0).\ k_1.\ t].$$

In the case of this first solution which results from interactions between the *S* and *F* phases, the residual volume fractions will also be noted as $\Sigma_I(S - F)$ and $\Phi_I(S - F)$.

Second solution (*Eq.* [2]): *self degradation of S phase.* The self-degraded fraction of the *S* phase is noted as y. The solution is

$$k_2.t = y/\Sigma_0\ [\Sigma_0 - y]$$

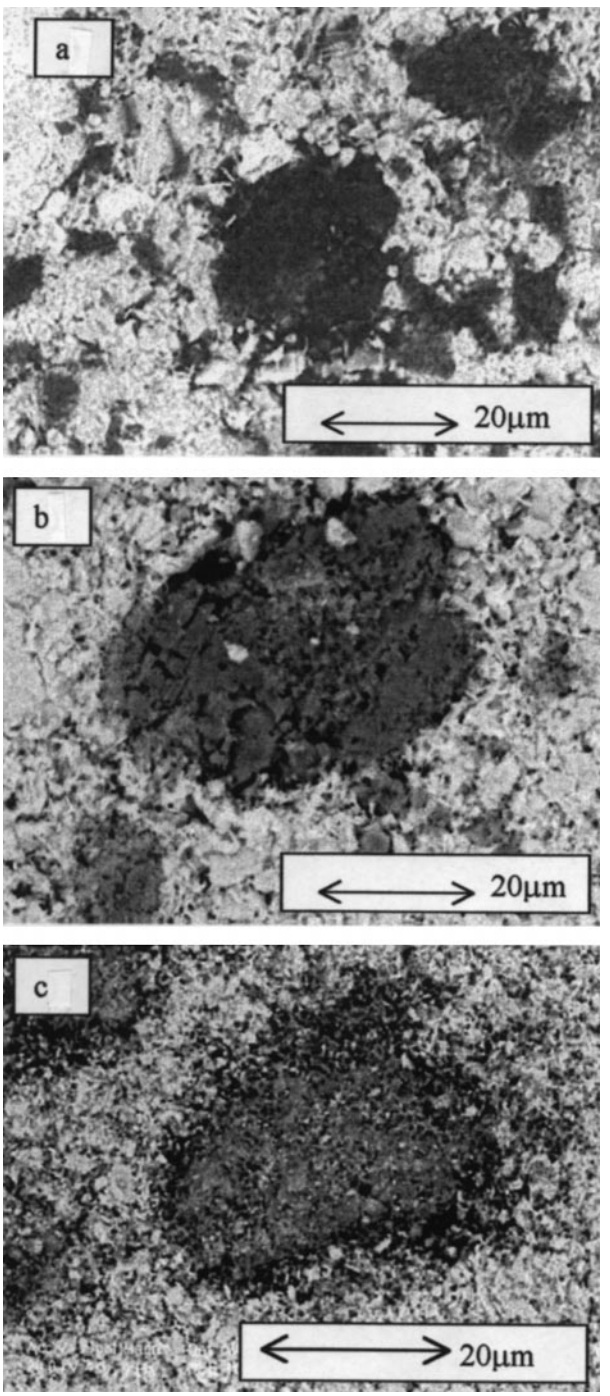

FIG. 6. Micrographs of the (a) S800, (b) S820, and (c) S830 composites for a vol. fraction Φ of 0.20.

which gives

$$y = k_2.\ t.\ \Sigma_0^2/[1 + k_2.t.\Sigma_0]$$

The residual volume fractions of S and F phases are noted as Σ_{II} and Φ_{II}. The two expressions can be derived as follows:

$$\Sigma_{II} = \Sigma_0 - y = \Sigma_0/[1 + k_2.t.\Sigma_0]$$

$$\Phi_{II} = 1 - \Sigma_0.$$

To interpret the evolution of the composites sintered at 830°C, Eq. [1] should be sufficient to represent our experimental data as a first approach. However, this unique equation [1] is not sufficient to correctly fit the experimental results. It is necessary to use a weighted combination of the two laws [1] and [2].

The residual volume fractions depend on the initial Φ_0 fraction and will then be calculated as follows:

$$\Sigma(\text{add}) = w_1\,.\,\Sigma_{I(S\text{-}F)} + w_2\,.\,\Sigma_{II(S\text{-}S)}$$

$$\Phi(\text{add}) = w_1\,.\,\Phi_{I(S\text{-}F)} + w_2\,.\,\Phi_{II(S\text{-}S)}$$

w_1 and w_2 being fitting weights depending on sintering temperature and time. However, the weighting factors w_i also depend on the initial ferrite composition Φ_0. To take into account the intermediate evolutions observed in the composition range [15 to 50%] in ferrite, we have assumed that these empirical w_i factors might be represented by:

$$w_1 = 1 - \exp(-(\Phi_0/f)^2)$$

and

$$w_2 = 1 - w_1 = \exp(-(\Phi_0/f)^2.$$

In these expressions, the f constant is a new fitting parameter representing the contribution of each type of reaction in our composites. Each f value should be connected with a typical fraction of ferrite above which the second reaction (Σ_{II} and Φ_{II} functions), corresponding to the self-degradation of the S phase, should be considered as negligible.

All the fitting parameters are summarized in Table 3.

The n value characterizes the type of chemical reaction and can be linked with the number of resulting reaction products at a given temperature. The observed limits Φ_{lim} are directly related to such a constant n. For $\Sigma_0 = 0$, one obtains $\Phi_{lim} = 1/n$. The k_1 and k_2 constants are characteristic of the reaction kinetics at a fixed temperature, n being known. It is thermally activated. The f factor gives the prominent reaction for a given fraction of ferrite.

TABLE 3
The Fitting Parameters of the Model

	Temperature [°C]		
Parameter	800	820	830
n	1.2 ± 0.2	3 ± 0.2	4.5 ± 0.2
k_1	$5.0 \times 10^{-3}\,s^{-1}$	$6.0 \times 10^{-3}\,s^{-1}$	$7.0 \times 10^{-3}\,s^{-1}$
k_2	$3.0 \times 10^{-5}\,s^{-1}$	$4.0 \times 10^{-5}\,s^{-1}$	$6.0 \times 10^{-5}\,s^{-1}$
f	0.65	0.40	0.30

If we consider the obtained n and k values, these parameters increase with the sintering temperature; this was expected because of the increase of decomposition phases (phase diagram). The f values are also in agreement with the limit Φ_{lim} values observed from the Bragg peak intensities (Figs. 2 and 7).

The modeled curves are reported in Figs. 7a–7c. The $\Sigma(\Sigma_0)$ and $\Phi(\Phi_0)$ functions are linked with the residual fractions of superconductor or ferrite phases. The x function describes the degradation process.

If the sole first model was used, the evolution of the S phase might well be represented, while the evolution of the ferrite phase would be poorly represented at low ferrite composition. If we use both models with the weighting factor f, we can have an acceptable simulation of the Φ and Σ functions.

It can be stated that, in the composition range 0 to 40 vol% of ferrite, a similar abnormal behavior is observed in the X-ray diffraction analyses of the residual fractions and in the evolution of the magnetic forces.

V. CONCLUSIONS

Taking into account the complex system involved in our composites, this simplified modeling can be considered as a first approach of the reaction sintering process in granular initially two-phase materials. It delivers three types of parameters for the sintering process in our composites:

- the value of n in the chemical equation which can be associated with the fast degradation of the Bi-2223 phase;
- the kinetics parameter k_1 which allows a definition of the degradation rate in the composite system;
- the kinetics parameter k_2 which characterizes the self degradation of the cuprate phase;
- the weighting parameter f which gives a first indication of the competition between the two degradation processes invoked above.

The first SEM analyses show that the (Bi, Sr, Ca, Cu) elements of the S phase quickly migrate and react with the

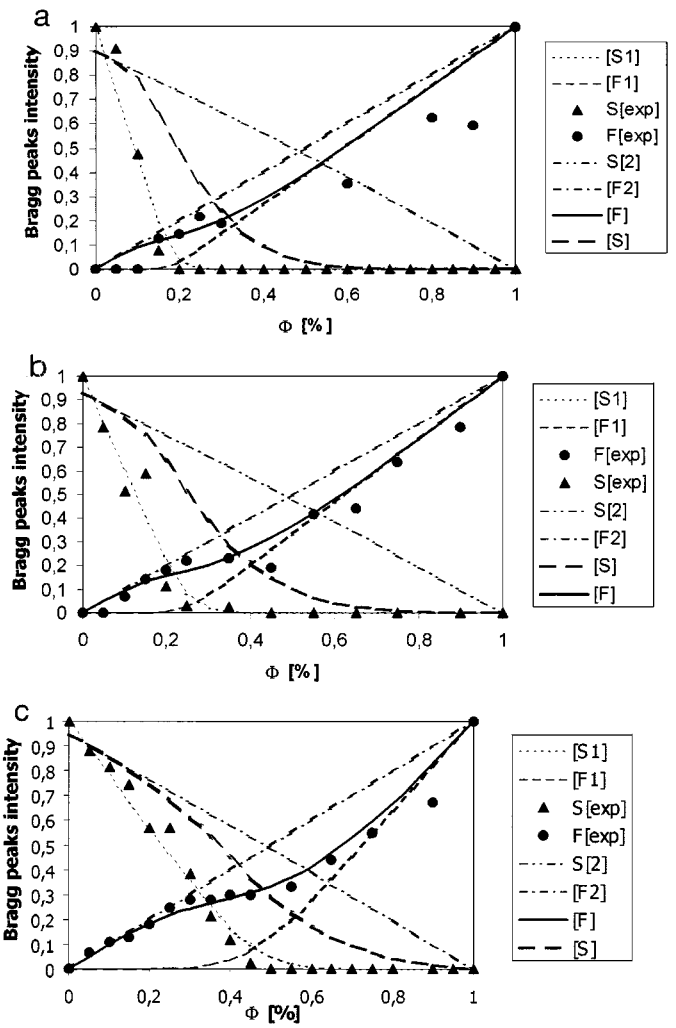

FIG. 7. Modeling of chemical kinetics in F/S composites: the total Σ and Φ functions are shown for each sintering temperature. The abnormal behavior in the Φ_0 range 0 to 0.40 is partly simulated. (a) S830 samples at 830°C; (b) S820 samples at 820°C; (c) S800 samples at 800°C.

ferrite grains. Correlatively, the migration of the Fe or Ni elements is less extended. These observations confirm the general form of our modeling. A detailed analysis is now in progress to correlate the present kinetics analysis with chemical diffusion coefficients.

REFERENCES

1. S. Jin, R. C. Sherwood, T. H. Tiefel, G. W. Kammlott, R. A. Fastnacht, M. E. Davis, and S. M. Zahurak, *Appl. Phys. Lett.* **52,** 1628 (1988).
2. M. Manzel, L. Illgen, and R. Hergot, *Phys. Status Solidi* (*A*) **117,** K119 (1990).
3. L. S. Hung, J. A. Agostinelli, G. R. Par-Pujalt, and J. M. Mir, *Appl. Phys. Lett*., **53,** 2450 (1988).
4. W. Gao and J. B. Vander Sande, *Physica C* **171,** 69 (1990).
5. R. H. Arendt, M. F. Garbauskas, K. W. Lay, and J. E. Tkaczyk, *Physica C* **194,** 383 (1992).
6. W. Gao and J. B. Vander Sande, *Mater. Sci. Eng. B* **10,** 247 (1990).
7. Y. Huang, G. F. De la Fuente, A. Sotelo, Physica C **185–189,** 2401 (1991)
8. Y. Ishida, J. Matsuzaki, T. Kizuka, and H. Ichionose, *Physica C* **190,** 67 (1991).
9. J. Koshy, K. S. Kumar, Y. P. Yadava, and A. D. Damodaran, *J. Mater. Sci. Lett*. **13,** 554 (1994).
10. Y. D. Chiu, T. S. Lei, and C. H. Kao, *J. Mater. Sci.* **29,** 2678 (1994).
11. R. Chaim and Y. Ezer, *J. Mater. Sci.* **28,** 4205 (1993).
12. R. Chaim and Y. Ezer, *J. Mater. Sci.* **28,** 5007 (1993).
13. R. Chaim and Y. Ezer, *J. Mater. Sci.* **28,** 4273 (1993).
14. In-Gan Chen, S. Sen, and D. M. Stefanescu, *Appl. Phys. Lett*. **52,** 1355 (1988).
15. G. Xiao, F. H. Streitz, M. Z. Cieplak, A. Bakhshai, A. Gavrin, and C. L. Chien, *Phys. Rev. B* **38,** 776 (1988).
16. R. K. Nkum, A. Punnett, and W. R. Datars, *Physica C*, **202,** 371 (1992).
17. C. Veerender and M. Nagabhooshanam, *J. Mater. Sci.* **30,** 369 (1995).
18. Y. Li and B. Yang, *J. Mater. Sci. Lett*. **13,** 594 (1994).
19. Y. Nishi, K. Nozaki, T. Kurotaki, Y. Kita, and K. Oguri, *J. Mater. Sci. Lett*. **11,** 1211 (1992).
20. Y. Nishi, K. Nozaki, T. Kurotaki, Y. Kita, and K. Oguri, *Ph. Lett. A* **163,** 465 (1992).
21. B. Ropers, F. Carmona, and S. Flandrois, *Physica C* **204,** 71 (1992).
22. B. Ropers, F. Carmona, and S. Flandrois, *Appl. Supercond*. **1**(7–8), 1015 (1993).
23. S. Dubois, S. Flandrois, and F. Carmona, *Phys. A* **207,** 265 (1994).
24. A. Ouammou, O. Pena, A. Benlhachemi, J. R. Gavarri, and C. Carel, *Ann. Chim. Fr*. **19,** 493–498 (1994).
25. A. Benlhachemi, J.R. Gavarri, Y. Massiani, and J. Marfaing, *Annal. Chim, Sci. Matér*. **20,** 335 (1995).
26. C. Alfred-Duplan, J. Marfaing, G. Vacquier, A. Benlhachemi, J. Musso, and J. R. Gavarri, *Mater. Sci. Engin. B* **29,** 1 (1996).
27. A. Benlhachemi, S. Golec, and J. R. Gavarri, *Physica C* **209,** 353 (1993).
28. A. Benlhachemi, J. Musso, J.R. Gavarri, C. Alfred-Duplan, and J. Marfaing, *Phys. C* **230,** 246 (1994).
29. A. Benlhachemi, J. R. Gavarri, J. Musso, C. Alfred-Duplan, and J. Marfaing, *Metall. Foundry Enging* **20,** 205 (1994).
30. A. Benlhachemi, J. R. Gavarri, Y. Massiani, and S. Aïtyazza, *Physica C* **235,** 1511 (1994).
31. A. Siwek, I. Suliga, M. H. Pischedda, J.R. Gavarri, and St. Jasienska, *Sol. Stat. Ionics* **80,** 45 (1995).
32. J. Schneck, J. C. Toledano, L. Pierre, A. Litzler, D. Morin, J. Primot, H. Savary, and C. Daguet, *J. Less Common Metals* **164,165,** 545 (1990).